5G ULTRA-DENSE NETWORKS WITH NON-UNIFORM DISTRIBUTED USERS

Junliang Ye[1], *Student Member, IEEE*, Xiaohu Ge[1], *Senior Member, IEEE*
Guoqiang Mao[2], *Senior Member, IEEE*, Yi Zhong[1], *Member, IEEE*

***Abstract*—User distribution in ultra-dense networks (UDNs) plays a crucial role in affecting the performance of UDNs due to the essential coupling between the traffic and the service provided by the networks. Existing studies are mostly based on the assumption that users are uniformly distributed in space. The non-uniform user distribution has not been widely considered despite that it is much closer to the real scenario. In this paper, Radiation and Absorbing model (R&A model) is first adopted to analyze the impact of the non-uniformly distributed users on the performance of 5G UDNs. Based on the R&A model and queueing network theory, the stationary user density in each hot area is investigated. Furthermore, the coverage probability, network throughput and energy efficiency are derived based on the proposed theoretical model. Compared with the uniformly distributed assumption, it is shown that non-uniform user distribution has a significant impact on the performance of UDNs.**

***Index Terms*—5G networks, radiation and absorbing model, small cell networks, user density.**

Submitted to IEEE Transactions on Vehicular Technology.
Correspondence author: Dr. Xiaohu Ge, Tel: +86 (0)27 87557941, Fax: +86 (0)27 87557941 Email: xhge@mail.hust.edu.cn.
The authors would like to acknowledge the support from the NFSC Major International Joint Research Project under the grant 61210002, National Natural Science Foundation of China (NSFC) under the grants 61301128 and 61461136004, the Ministry of Science and Technology (MOST) of China under the grants 2014DFA11640 and 2012DFG12250, the Fundamental Research Funds for the Central Universities under the grant 2015XJGH011, the Special Research Fund for the Doctoral Program of Higher Education (SRFDP) under grant 20130142120044. This research is partially supported by the EU FP7-PEOPLE-IRSES, project acronym S2EuNet (grant no. 247083), project acronym WiNDOW (grant no. 318992) and project acronym CROWN (grant no. 610524).

I. INTRODUCTION

A. Related works

The fifth generation (5G) mobile communication systems are envisaged to provide a 1000 times enhancement of the network capacity while achieving a much higher energy efficiency compared with the fourth generation (4G) mobile communication systems. The ambitious aims of 5G mobile communication systems bring both opportunities and challenges to researchers all over the world [1]. The UDNs are regarded as one of the key technologies for 5G mobile communication systems [2]. The main difference between UDNs and heterogeneous networks (HetNets) lies in the dramatic increase of small cell base station (SBS) density. The distances between users and SBSs are greatly reduced with the increase of the SBS density, hence more wireless links are available for users in wireless networks to enhance the quality of service (QoS) [3]. On the other hand, UDNs also suffer from the increasing energy consumption with the massive deployment of SBSs. Therefore, one of the core problems for deploying UDNs is the optimization of SBS density to meet the traffic demand in an energy efficient way in hot spot areas.

Some recently studies were conducted to evaluate the performance of UDNs. A basic question was investigated in [4]: how to choose the SBS density for a 5G UDN when the backhaul capacity and energy efficiency are jointly considered. A comprehensive introduction of researches about the energy efficiency of UDNs was given by G. Wu et al. and the tradeoff between energy efficiency and spectrum efficiency was highlighted in [5]. A resource allocation scheme was proposed to analyze trade-offs between the spectrum efficiency and energy efficiency of 5G UDNs [5]. The influence of SBS density on the outage probability was discussed and different multiple access technologies were compared to obtain the optimal solutions for allocating subcarriers with interference constraints [6]. The Lyapunov method and mean field game were utilized to optimize the energy efficiency with the QoS constraints [7]. The impact of the spectrum bandwidth and SBS density on the capacity and the spectrum efficiency

was analyzed in [8]. Comparisons between different spectrum bandwidths and SBS densities were made by D. Lpez-Prez et al. to propose a technique for increasing the average user capacity to 1 gigabit per second (Gbps) [8]. Cognitive radio technologies were adopted to enhance the throughput of 5G UDNs [9], and energy efficient optimal power allocation strategies subject to constraints on the average interference power are proposed in [10]. On the other hand, the stochastic geometry theory is widely used to evaluate the performance of UDNs. The delay of heterogeneous cellular networks with spatial temporal traffic was investigated by using stochastic geometry in [11]. Closed-form formulas of network capacity and energy efficiency were derived in [12] by modeling the wireless network using the stochastic geometry tools. The difference between line of sight (LoS) channel and non-line of sight (NLoS) channel was considered to evaluate the impact of channel fading on the spatial spectrum efficiency [13]. It was shown in [13] that the network spatial spectrum efficiency will not monotonously increase with the increase of the SBS density when LoS and NLoS channels are considered. A new type of UDNs including femtocell base stations (FBSs), macro cell base stations (MBSs) with distributed antennas was proposed in [14], where the energy efficiency, spectrum efficiency and spatial spectrum efficiency of UDNs were improved. By utilizing an innovative millimeter-wave (mmWave) decoupling method, mmWave can be used by network users for uplink transmissions to traditional microwave base stations (BSs) [15]. Based on the mmWave decoupling method, a closed-form formula for spectrum efficiency of UDNs was derived and a resource management method was proposed to optimize downlink transmission rate of UDNs with a minimum uplink rate constraint. The backhaul traffic of UDNs based on the mmWave and massive MIMO technologies was analyzed and the impact of different pre-coding methods was also investigated in [16]. When both the long-term evolution (LTE) and the wireless fidelity (WiFi) were deployed in UDNs, a Markov chain model was utilized to analyze the performance of the proposed LTE-WIFI UDNs [17]. Based on the energy harvesting technology, the trade-off between the energy efficiency and the QoS was analyzed for UDNs [18]. Furthermore, a fractional programming method was adopted to investigate the energy efficiency maximization problem of wireless networks under a minimum system throughput constraint [19].

Though the aforementioned studies have investigated many aspects of UDNs, most of them only focused on studying the influence of SBS density on the capacity and energy efficiency. Few effort has been spent on the effect of the SBS density on both the network performance and the user experiences simultaneously. Recently, the virtual cell technology has been widely used to improve the user experience of UDNs [20]–[25]. By adopting the virtual cell technology, a new type of UDNs termed user-centric UDNs were introduced in [20]. The main idea of user-centric UDNs is to cluster SBSs dynamically and intelligently to provide better services for users. Based on virtual cells in UDNs, a new type of beam forming technology named the balanced beam forming algorithm was developed to optimize the network capacity [21]. A type of virtual cell networks based on distributed antennas were presented in [22], and the influence of cell size on the users' maximum downlink achievable rate was investigated. Based on stochastic geometry theory, the trade-off between the energy efficiency and spectrum efficiency of UDNs was investigated to optimize the energy efficiency with the minimum network capacity constraints [23]. By the joint optimization of virtual cell clustering method and the beam forming algorithm, the sum capacity was improved for UDNs [24]. By optimizing the interference nulling range, the user-centric interference nulling method was proposed in [25], where the outage probability is reduced by 35%–40%.

B. Main contributions

From the above discussion, one can observe that the focus of the researches on UDNs turns from network performance to user experience. Moreover, the design and optimization of UDNs develops from network-centric to user-centric. Due to uncertainties of users' activities, few work have studied the impact of users' activities on the network performance . By measuring the entropy of each individual's moving trajectory, Song et al. found a 93% potential predictability in user mobility [26]. Based on the human mobility trajectory measured from real data, the individual mobility model considering the human mobility tendency habit was proposed to describe the human mobility in the real world [27]. The gravity law model was established to analyze the number of commuters between different areas [28]. The theoretical result of [28] was improved in [29]. By proposing the Radiation and Absorbing (R&A) model and comparing it with the empirical data, the R&A model was proved to be highly reliable in large range of spatial scale. Although there exist a large amount of meaningful and important studies for UDNs, one basic question is still not well answered: how many SBSs are required to meet the greatly increased traffic demand while guaranteeing a high energy efficiency? To answer this question, a theoretical model including user density, BS deployment, interference analysis and energy consumption need to be established for 5G UDNs. Based on this unsolved problem, the contributions and novelties of this paper are summarized as follows.

1) Based on the queueing network theory, the R&A model is first used to analyze the effect of the user density on the performance of 5G ultra-dense small cell networks in the temporal domain.
2) By utilizing the integral geometry and Euler summation, the impact of user and SBS densities on the coverage probability and average number of SBSs in virtual cells is investigated. Furthermore, by adopting a two-dimensional Markov chain, the blocking probability and channel occupancy rate are analyzed for 5G ultra-dense small cell networks based on the R&A model.
3) Based on the theoretical analysis on channel capacity and energy consumption of 5G ultra-dense small cell networks, the network energy efficiency is investigated using the proposed models. Simulation results indicate that the non-uniformly distribution of users has a profound effect on the energy efficiency.

The rest of this paper is organized as follows. Section II describes the system model of 5G UDNs. The R&A model is introduced in section II-A, then the model is extended by the queueing network theory in section II-B. The interference model and the SBS service model are described in section II-C and section II-D, respectively. Network performance metrics are analyzed and derived in Section III. Numerical and simulation results are displayed in section IV. Finally, Section VI concludes this paper.

II. System Model

A. Radiation and Absorbing model

Definitions of some default parameters are shown in the following table.

TABLE I
An Example of a Table

$\mathrm{HS_i}$	Hot spot i
$\mathrm{CR_i}$	Coverage region of $\mathrm{HS_i}$
S_i	Coverage area of $\mathrm{CR_i}$
l_i	Radius of $\mathrm{CR_i}$
P_i	Number of users in $\mathrm{CR_i}$
$N_S\left(i\right)$	Number of SBSs in $\mathrm{CR_i}$
m_i	Attraction exponent of $\mathrm{HS_i}$
T_{ij}	Number of moving users from $\mathrm{HS_i}$ to HS_j
U_{HS_i}	Typical user of $\mathrm{HS_i}$
S_{HS_i}	Typical SBS of $\mathrm{HS_i}$

In this paper, the R&A model is used to analyze the distribution of mobile users in a two dimension plane $\mathbb{R}^2$. Let $\mathbb{A}_T$ be a region with area S_A on the plane $\mathbb{R}^2$. The places with large number of users are denoted as hot spots in $\mathbb{A}_T$. The set of hot spots is denoted by Υ, the cardinality of Υ is N_p and elements of Υ are denoted by $\{\mathrm{HS_i}|1 \leq i \leq N_p\}$. The system QN is defined as a set formed by all users, hot spots and SBSs in $\mathbb{A}_T$. The coverage region of the hot spot $\mathrm{HS_i}$ is denoted by CR_i which is assumed to be a circle with a radius l_i. Thus, the area of CR_i is $S_i = \pi l_i^2$. According to the definition of the R&A model, users can commute with all other hot spots in $\mathbb{A}_T$. The probability that one user moves from $\mathrm{HS_i}$ to HS_j is denoted as r_{ij} and expressed as follow [29].

$$r_{ij} = \frac{m_i m_j}{\left(m_i + s_{ij}\right)\left(m_i + m_j + s_{ij}\right)}, \tag{1}$$

where m_i and m_j are attraction exponents (AEs) of $\mathrm{HS_i}$ and HS_j, respectively. Based on the definition in the supplementary material of [29], AEs are configured as fixed values determined by several parameters like the number of available jobs, average salary and consumption level of the corresponding hot spot. s_{ij} denotes the total value of AEs (excluding AEs of $\mathrm{HS_i}$ and HS_j) in the circle centered at $\mathrm{HS_i}$ with radius l_{ij}, where l_{ij} is the distance between the centers of $\mathrm{HS_i}$ and HS_j.

The total number of users commuting from $\mathrm{HS_i}$ to HS_j during Δt is denoted by T_{ij}. Then, T_{ij} is a binomial random variable by assuming moving characteristics of different users inside the QN system are independent from each other. The expectation of T_{ij} is

$$\mathbb{E}\left(T_{ij}\right) = \zeta P_i \frac{m_i m_j}{\left(m_i + s_{ij}\right)\left(m_i + m_j + s_{ij}\right)}, \tag{2}$$

where $\mathbb{E}\left(\cdot\right)$ is the expectation operation. The ratio of moving users in the total population is configured as a fixed value denoted by ζ.

B. Queueing Network Model

Based on the definition in [29], the original R&A model is only used for the theoretical analysis in the spatial domain. Thus, to evaluate the stationary number of users in the coverage region of each hot spot in the QN system, the queueing network model is adopted in this paper to extend the R&A model to the temporal domain. We assume that all users in the coverage region of a hot spot are stayed in a queue so that the number of users in the coverage region is equal to the length of the corresponding queue. Furthermore,

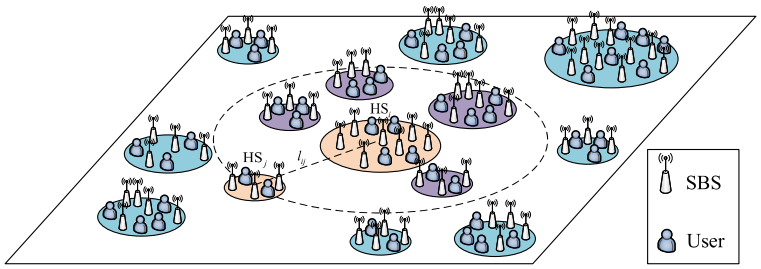

Fig. 1. System model. Coverage areas of different hot spots are shown as circles with different radius, s_{ij} is the total number of AEs in circles marked as the purple regions.

users in the queue are assumed to be served by a server in the corresponding hot spot, and a user will leave the hot spot after the user is served. Thus, the arrival rate and serving rate of a queue are evaluated by the expected number of users that moving in and out of the hot spot respectively during a given time slot Δt.

The Jackson network (JN) is a basic type of queueing networks. Based on the definition of JN [30], users outside of a queueing network system may move into a hot spot contained in the queueing network system. Fig. 2 is a Jackson network system (JNS) formed by two queues.

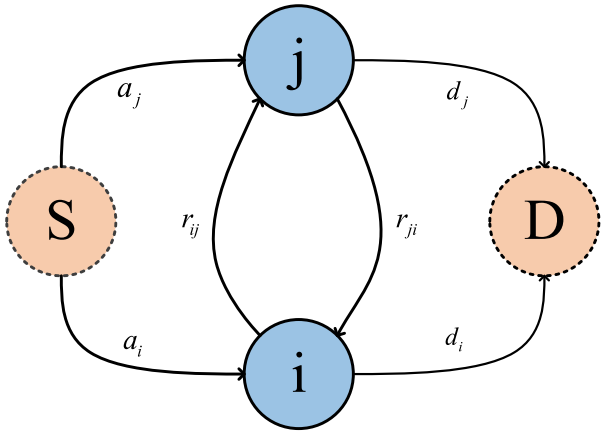

Fig. 2. An example of JNS that contains two queues i and j. Users outside of JNS are denoted by S, and users exiting from JNS are denoted by D. The probability that a user transfers from S to i and j is a_i and a_j. The probability that a user leaves the JNS from i (j) is d_i (d_j). The probabilities that a user moves between i and j are denoted by r_{ij} and r_{ji}, respectively.

In this paper, the number of users in CR_i at time t is denoted as P_i. Based on the definition of JN in [30], P_i is independent from the length of other queues in the QN system. The serving rate of the queue in $\mathrm{HS_i}$ is denoted as μ_i. In the QN system, the stationary value of P_i exists if the condition $\rho_i = \frac{\lambda_i}{\mu_i} < 1$ is satisfied. The QN system keeps a stationary state when lengths of all queues in the QN system remain stationary.

C. Interference Model

In this paper, all SBSs and users of $\mathrm{HS_i}$ are assumed to be randomly and uniformly distributed in CR_i. Furthermore, an typical user in CR_i is donated by U_{HS_i} and an typical SBS in CR_i is denoted as S_{HS_i}. The distance between U_{HS_i} and S_{HS_i} is denoted by l_{mc}. Based on the result in [31], we have

$$f_{l_{mc}}(x) = \frac{4x}{\pi l_i^2}\left(\arccos\frac{x}{2l_i} - \frac{x}{2l_i}\sqrt{1-\frac{x^2}{4l_i^2}}\right), \quad (3)$$

where $f_{l_{mc}}(x)$ is the probability density function (PDF) of the random variable l_{mc}. In this paper, the function $f_X(\cdot)$ is used to denote the PDF of a random variable X.

The orthogonal frequency division multiplexing (OFDM) technology is assumed to be adopted by all SBSs in the QN system. In this paper, SBSs that transmit useful signals to users are called the associated SBSs while SBSs that generate interference are called interfering SBSs. Users are assumed to receive downlink interference only from SBSs within the same hot spot with them. The small scale fading of all channels are assumed to be governed by independent and identically distributed (*i.i.d.*) Rayleigh distributions. By ignoring the shadowing, the coverage probability of S_{HS_i} to U_{HS_i} is expressed by

$$P_{\text{cover}} = \Pr\left(\frac{p_t G_s R_s^{-\alpha_p}}{\sigma^2 + \sum_{i=0}^{\overline{N_{\text{int}}}} p_t G_i R_i^{-\alpha_p}} \geq \gamma_0 \right), \quad (4)$$

where $\Pr(\cdot)$ is the probability corresponding to the expression in parentheses, γ_0 is the threshold of the received signal to interference plus noise ratio (SINR) at user devices, p_t is the transmit power consumption of a SBS, σ^2 is the power of the additive white Gaussian noise (AWGN), α_p is the path loss exponent, $\overline{N_{\text{int}}}$ is the average number of interfering SBSs, R_s is the distance between a user and an associated SBS, R_i is the distance between a user and an interfering SBS, G_s and G_i are the small scale fading experienced by the desired link and interfering links, respectively. Based on the assumption that small scale fading of all channels follows *i.i.d.* Rayleigh distributions, G_s and G_i are exponential distributed random variables with expectations η.

The event that a user is covered by a SBS is assumed to be independent of the event that the user is covered by another SBS. Thus, the number of SBSs that cover the same user is a binomial distributed random variable. The expectation of the binomial distributed random variable is

$$\mathbb{E}(N_{\text{cover}}) = \overline{N_{\text{cover}}} = N_S(i) P_{\text{cover}}. \quad (5)$$

All SBSs that can cover a same user are configured to form a virtual cell cluster (VC). SBSs in a VC are assumed to be able to transmit signals to the served user simultaneously without causing interference [3]. Thus, the number of interfering SBSs is

$$\overline{N_{\text{int}}} = N_{\text{SBS}} - \overline{N_{\text{cover}}} = N_S(i)(1 - P_{\text{cover}}). \quad (6)$$

By substituting (6) into (4), the coverage probability is further derived by

$$P_{\text{cover}} = \Pr\left(\frac{p_t G_s R_s^{-\alpha_p}}{\sigma^2 + \sum_{i=0}^{N_S(i)(1-P_{\text{cover}})} p_t G_i R_i^{-\alpha_p}} \geq \gamma_0 \right). \quad (7)$$

D. Channel Access Model

A channel is called an available channel if the received SINR at the user using this channel is larger than a given threshold γ_0. A user will be blocked when all available channels of the associated SBS are occupied. Thus, a two-dimensional Markov chain is utilized to analyze channel access processes of SBSs in the QN system [32]. Two states of the two-dimensional Markov chain are denoted by (v_m, v_n), where v_m denotes the number of occupied channels in a SBS and v_n is the number of available channels in a SBS ($v_m \leq v_n$), respectively.

The probability that a user has a downlink communication request to a SBS is denoted by p_s. Communication requests of different users are assumed to be *i.i.d.*. Thus, the number of users with communication requests follows a binomial distribution with expectation $\overline{P_i} \cdot p_s$, where $\overline{P_i}$ is the stationary number of users in CR_i. Since $\overline{P_i}$ is usually a large value, the binomial distribution can be approximated by a Poisson distribution with the same expectation $\overline{P_i} \cdot p_s$. The call arriving process of S_{HS_i} is denoted by AP and the number of calls arriving at S_{HS_i} before time t is denoted by $\text{AP}(t)$. Thus, we have the following equation

$$\Pr\{\text{AP}(t+\Delta t) - \text{AP}(t) = n\} = e^{-\frac{\overline{P_i} \cdot p_s \Delta t}{N_S(i)}} \frac{\overline{P_i} \cdot p_s (\Delta t)^n}{n! N_S(i)}. \quad (8)$$

The call arriving process of S_{HS_i} is supposed to be a stochastic process with independent and stationary increments. Thus, the stochastic process AP is a Poisson process. The value of the serving duration of S_{HS_i} to U_{HS_i} is assumed to be an exponential distributed random variable with expectation μ_s. The corresponding transition diagram of the two-dimensional Markov chain is shown as follows.

The transition diagram of the two-dimensional Markov chain is explained as follows.

1) $(v_m, v_n) \to (v_m + 1, v_n)$: A user has been successfully allocated an available idle channel of S_{HS_i}, then $v_m + 1$.
2) $(v_m, v_n) \to (v_m, v_n + 1)$: An unavailable channel of S_{HS_i} becomes available due to the time-varying interference, thus $v_n + 1$.
3) $(v_m, v_n) \to (v_m - 1, v_n)$: A user has been fully served and releases the occupied channel of S_{HS_i}, then $v_m - 1$.
4) $(v_m, v_n) \to (v_m, v_n - 1)$: An available channel of S_{HS_i} becomes unavailable due to the time-varying interference, thus $v_n - 1$.

The maximum number of available channels offered by S_{HS_i} is denoted as C. The transition rate for an unavailable channel becoming available is denoted by α_s, and the transition rate for an available channel becoming unavailable is denoted by β_s. The call arriving rate $\lambda_{i,s}$ is

$$\lambda_{i,s} = \frac{\overline{P_i} \cdot p_s \cdot \overline{N_{\text{cover}}}}{N_S(i)}. \quad (9)$$

Based on the Kolmogorov criteria [32], the two-dimensional Markov chain in Fig. 3 is reversible and the stationary state distribution of the two-dimensional Markov chain exists.

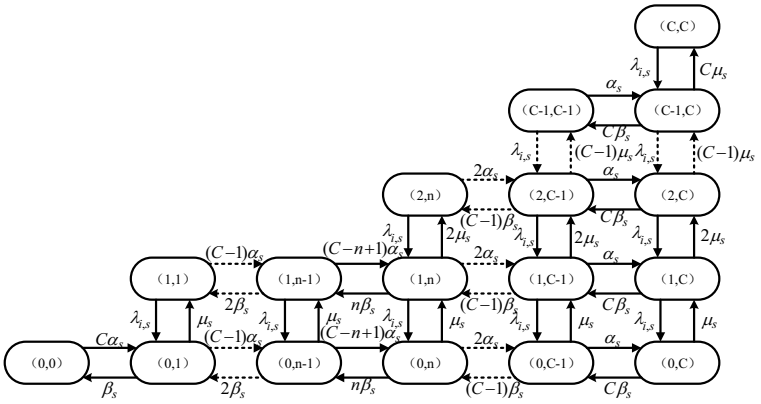

Fig. 3. Transition diagram of the two-dimensional Markov chain.

III. Coverage Probability, Blocking Probability and Throughput

A. Coverage Probability

The coverage probability in (7) can be further evaluated as (10).

$$\begin{aligned} P_{\text{cover}} &= \Pr\left(\frac{p_t G_s R_s^{-\alpha_p}}{\sigma^2+\sum_{i=0}^{N_S(i)(1-P_{\text{cover}})} p_t G_i R_i^{-\alpha_p}} \geq \gamma_0\right) \\ &= \Pr\left(\frac{G_s}{\frac{1}{\rho_0}+\frac{\sum_{i=0}^{N_S(i)(1-P_{\text{cover}})} G_i R_i^{-\alpha_p}}{R_s^{-\alpha_p}}} \geq \gamma_0\right) \\ &= \Pr\left(\frac{1}{\rho_0 G_s}+\frac{\sum_{i=0}^{N_S(i)(1-P_{\text{cover}})} G_i R_i^{-\alpha_p}}{G_s R_s^{-\alpha_p}} \leq \gamma_0^{-1}\right), \end{aligned} \tag{10}$$

where ρ_0 is the received signal to noise ratio (SNR) of U_{HS_i}. The expression of ρ_0 is

$$\rho_0 = \frac{p_t R_s^{-\alpha_p}}{\sigma^2}. \tag{11}$$

Based on the result in [33], ρ_0 is configured as a determined variable in this paper.

Based on (10) and (11), the coverage probability P_{cover} is finally derived as

The corresponding derivation and explanation is shown in the appendix A.

B. Blocking Probability

By the definition of JN in [30], a QN system should meet the following three necessary conditions for being a JN:

1) User arriving processes in all hot spots are independent Poisson processes in the QN system
2) Users outside of the QN system can move into the QN system.
3) Users who are fully served in the QN system can either move to another hot spot in the QN system or leave the QN system.

Denote the total number of users moving from outside of $\mathbb{A}_T$ into CR_i during a time period Δt as e_i. By assuming e_i as a random variable with expectation a_i, we get the following lemmas.

Lemma 1: For a large P_i, the binomial distributed random variable T_{ij} can be approximated by a Poisson distributed random variable with the expectation being $\mathbb{E}(T_{ij})$.

The number of users in a hot spot is modeled by a queueing network model in the temporal domain. Based on the definition of JN users who have been fully served in a hot spot either choose to be added into another queue or to leave the queueing network [30]. Based on the above model, we get the following Lemma 2.

Lemma 2: Based on Lemma 1 and the assumption that e_i is a Poisson distributed random variable, the number of users moving into CR_i during Δt is a Poisson distributed random variable. The expectation of the number of users moving into CR_i during Δt is

$$\lambda_i = a_i + \sum_{j\in(1,N_p),j\neq i} \mathbb{E}(T_{ji}). \tag{13}$$

Lemma 3: Assuming numbers of users moving into CR_i during each disjoint Δt in the temporal domain are *i.i.d.*. Thus, the user arriving process of HS_i is a stochastic process with independent and stationary increments.

By combining Lemma 1, Lemma 2 and Lemma 3, the user arriving process of HS_i is proved to be a Poisson process.

$$P_{\text{cover}} = 2^{-B_e}\gamma_0 \exp\left(\frac{A_e}{2}\right) \sum_{b_e=0}^{B_e} \left(\begin{array}{c} B_e \\ b_e \end{array} \right) \sum_{c_e=0}^{C_e+b_e} \frac{(-1)^{c_e}}{D_e} \times \\ \text{Re}\left(\left(\int_0^{\infty} \left(\eta \exp\left(-\frac{\hbar}{\rho_0 G_s} - \eta G_s \right) \left(\int_0^{\infty} \int_0^{2l_i} \int_0^{2l_i} \exp\left(\frac{-\hbar G_i R_i^{-\alpha_p}}{G_s R_s^{-\alpha_p}} \right) \left(\frac{4R_s}{\pi l_i^2} \left(\arccos \frac{R_s}{2l_i} - \frac{R_s}{2l_i} \sqrt{1 - \frac{{R_s}^2}{4l_i^2}} \right) \right) \times \right. \right. \right. \right. \\ \left. \left. \left. \left. \left(\frac{4R_i}{\pi l_i^2} \left(\arccos \frac{R_i}{2l_i} - \frac{R_i}{2l_i} \sqrt{1 - \frac{{R_i}^2}{4l_i^2}} \right) \right) \left(\eta \exp\left(-\eta G_i \right) \right) dG_i dR_s dR_i \right)^{\overline{N_{\text{int}}}} \right) dG_s \right) / \hbar \right). \tag{12}$$

Then, we get the following theorem.

Theorem 1: Assuming users' moving actions among different hot spots are governed by a R&A model. By denoting the number of users in each hot spot as the size of the corresponding queue, the QN system can be modeled by a Jackson network.

The transferring matrix of the QN system is denoted by $\mathbf{R}$. The element of the matrix $\mathbf{R}$ located at the row i and the line j is denoted as $[\mathbf{R}]_{ij}$, which is the probability that a user moves from HS_i to HS_j. Thus, $[\mathbf{R}]_{ij}$ is expressed by

$$[\mathbf{R}]_{ij} = \begin{cases} \frac{m_i m_j}{(m_i + s_{ij})(m_i + m_j + s_{ij})} & 0 < i \neq j \leq N_p \\ 0 & 0 < i = j \leq N_p \end{cases}. \tag{14}$$

The probability that a user leaves the QN system from HS_i is

$$d_i = 1 - \sum_{j=1}^{N_p} [\mathbf{R}]_{ij}. \tag{15}$$

When the QN system is in a stationary state the number of users leave the QN system from HS_i during Δt is denoted as $\overline{D_i}$ with expectation as follows.

$$\mathbb{E}\left(\overline{D_i}\right) = \zeta \overline{P_i}, \tag{16}$$

where $\overline{P_i}$ denotes the stationary number of users in CR_i. Substitute (14) and (16) into (2), the expectation of the number of users moving into CR_i during Δt is

$$\lambda_i = a_i + \sum_{j \in (1, N_p), j \neq i} \lambda_j r_{ji}. \tag{17}$$

To keep the stability of the total number of users in the QN system, a_i is configured as

$$a_i = \zeta \frac{\sum_{i=1}^{N_p} m_i d_i}{N_p} = \zeta \frac{\sum_{i=1}^{N_p} m_i \left(1 - \sum_{j=1}^{N_p} [\mathbf{R}]_{ij} \right)}{N_p}. \tag{18}$$

By denoting $\mathbf{a} = \left(a_1, a_2, \ldots, a_{N_p}\right)_{1 \times N_p}$ and $\boldsymbol{\lambda} = \left(\lambda_1, \lambda_2, \ldots, \lambda_{N_p}\right)_{1 \times N_p}$, (28) is further derived by a matrix form as

$$\boldsymbol{\lambda} = \mathbf{a}(\mathbf{I} - \mathbf{R})^{-1}, \tag{19}$$

where $\mathbf{I}$ is an identical matrix. Based on (19), the user arriving rate of each hot spot can be obtained.

The stationary serving rate of the queue in HS_i is denoted as μ_i. By substituting λ_i into $\rho_i = \frac{\lambda_i}{\mu_i} = \frac{\lambda_i}{\zeta \overline{P_i}}$, the number of users in the stable status in CR_i is

$$\overline{P_i} = \frac{\rho_i}{1 - \rho_i} = \frac{\lambda_i}{\zeta \overline{P_i} - \lambda_i}. \tag{20}$$

By solving the implicit function in (11), $\overline{P_i}$ is further derived by

$$\overline{P_i} = \sqrt{\left(\frac{\lambda_i}{2\zeta} \right)^2 + \frac{\lambda_i}{\zeta}} + \frac{\lambda_i}{2\zeta}. \tag{21}$$

The stationary distribution of the state (v_m, v_n) in the two-dimensional Markov chain in Fig. 3 is denoted by $\pi\left(v_m, v_n\right)$. Based on the result in [32], $\pi\left(v_m, v_n\right)$ is expressed by (22) where $\left(\begin{array}{c} C \\ v_n \end{array} \right)$ is a binomial coefficient denoting the number of ways to pick v_n unordered outcomes from C possibilities. By the Gilbert-Elliott model [32], we have

$$\frac{\alpha_s}{\beta_s} = \frac{1 - \varepsilon_s}{\varepsilon_s}, \tag{23}$$

where ε_s is expressed as (35) and p_{oc} is the probability that a channel of S_{HS_i} is occupied.

$$\varepsilon_s = \sum_{\Delta_s=0}^{\overline{N_{\text{int}}}} \left(1 - P_{\text{cover}}\right) \left(\begin{array}{c} \overline{N_{\text{int}}} \\ \Delta_s \end{array} \right) \left(p_{\text{oc}}\right)^{\Delta_s} \left(1 - p_{\text{oc}}\right)^{\overline{N_{\text{int}}} - \Delta_s}, \tag{24}$$

By assuming U_{HS_i} accesses each channel with equal probability, the probability that a channel of S_{HS_i} is occupied is

$$p_{\text{oc}} = \sum_{v_m=0}^{v_n} \sum_{v_n=0}^{C} \frac{v_m}{C} \pi\left(v_m, v_n\right). \tag{25}$$

$$\pi\left(v_m, v_n\right) = \begin{cases} \frac{1}{\chi}\left(\frac{\lambda_{i,s}}{\mu_s}\right)^{v_m}\frac{1}{v_m!}\begin{pmatrix} C \\ v_n \end{pmatrix}\left(\frac{\alpha_s}{\beta_s}\right)^{v_n} \\ \chi = \sum\limits_{v_m \le v_n \le C}\left(\frac{\lambda_{i,s}}{\mu_s}\right)^{v_m}\frac{1}{v_m!}\begin{pmatrix} C \\ v_n \end{pmatrix}\left(\frac{\alpha_s}{\beta_s}\right)^{v_n} \end{cases}, \tag{22}$$

By substituting (23) (24) (25) into (22), the stationary probability $\pi\left(v_m, v_n\right)$ of the state $\left(v_m, v_n\right)$ is obtained. The call blocking probability of U_{HS_i} is

$$P_B = \sum_{v_m = v_n \le C} \pi\left(v_m, v_n\right). \tag{26}$$

By (22) and (26), the probability that U_{HS_i} is served by S_{HS_i} is derived as

$$\begin{aligned} P_{\mathrm{serve}} &= 1 - P_B \\ &= 1 - \sum_{v_m = v_n \le C} \frac{1}{\chi}\left(\frac{\lambda_{i,s}}{\mu_s}\right)^{v_m}\frac{1}{v_m!}\begin{pmatrix} C \\ v_n \end{pmatrix}\left(\frac{\alpha_s}{\beta_s}\right)^{v_n}. \end{aligned} \tag{27}$$

The probability that all channels of S_{HS_i} are idle is P_{idle}, given by

$$P_{\mathrm{idle}} = \sum_{v_n = 0}^{C} \pi\left(0, v_n\right). \tag{28}$$

C. Network Throughput

Based on the transition diagram of the two-dimensional Markov Chain in Fig. 3, the average number of occupied channels at S_{HS_i} is

$$\overline{N_{\mathrm{oc}}} = \sum_{v_m = 0}^{v_n}\sum_{v_n = 0}^{C} v_m \pi\left(v_m, v_n\right). \tag{29}$$

We assume that the transmission rate is assumed to be equal to the channel capacity when the channel is occupied. Thus, the stationary throughput of S_{HS_i} is

$$\begin{aligned} T_s &= \overline{N_{\mathrm{oc}}} \cdot \left(C_{ca}\right) \\ &= \left(C_{ca}\right)\sum_{v_m = 0}^{v_n}\sum_{v_n = 0}^{C} v_m \pi\left(v_m, v_n\right), \end{aligned} \tag{30}$$

By assuming the throughputs of all SBSs in the QN system are *i.i.d.*, the throughput of the small cell network restricted in CR_i is (31).

$$\begin{aligned} T_{\mathrm{HS}_i} = N_S\left(i\right)\left(\int_{x=\gamma_0}^{\infty}\log_2\left(1+x\right) f_{\lambda}\left(x\right) dx\right) \times \\ \sum_{v_m = 0}^{v_n}\sum_{v_n = 0}^{C} v_m \pi\left(v_m, v_n\right). \end{aligned} \tag{31}$$

The throughput of the small cell network in the QN system is (32).

$$\begin{aligned} T_{\mathrm{QN}} = \sum_{i=1}^{N_p} N_S\left(i\right)\left(\int_{x=\gamma_0}^{\infty}\log_2\left(1+x\right) f_{\lambda}\left(x\right) dx\right) \times \\ \sum_{v_m = 0}^{v_n}\sum_{v_n = 0}^{C} v_m \pi\left(v_m, v_n\right). \end{aligned} \tag{32}$$

D. Energy Efficiency

The total power consumption p_{to} of a SBS s_{ori} is [36]

$$p_{\mathrm{to}} = N_{\mathrm{oc}}\frac{\frac{p_t}{\eta_{\mathrm{pa}}} + p_{\mathrm{rf}} + p_{\mathrm{bb}}}{\left(1-\sigma_{\mathrm{dc}}\right)\left(1-\sigma_{\mathrm{ms}}\right)} + p_{\mathrm{st}}, \tag{33}$$

where p_t is the transmit power consumption of s_{ori}, η_{pa} is the efficiency coefficient of the power amplify module, p_{rf} is the power consumption of the radio frequency module, p_{bb} is the power consumption of the base band module, σ_{dc} is the loss coefficient of the digital control module, σ_{ms} is the power supply loss coefficient, p_{st} is the constant power consumption which is independent from the traffic load of s_{ori}, and N_{oc} is the number of occupied channels at s_{ori}, respectively. Based on the configuration in [36], the values of σ_{ms} and σ_{dc} are smaller than 1.

We assume that all SBSs are able to be shut down and turned on instantaneously without delay. Thus, the energy consumption of S_{HS_i} is

$$\begin{aligned} E_{to} = \left(\sum_{v_m = 1}^{v_n}\sum_{v_n = 1}^{C} v_m \pi\left(v_m, v_n\right)\frac{\frac{p_t}{\eta_{\mathrm{pa}}} + p_{\mathrm{rf}} + p_{\mathrm{bb}}}{\left(1-\sigma_{\mathrm{dc}}\right)\left(1-\sigma_{\mathrm{ms}}\right)} + p_{\mathrm{st}}\right) \times \\ \left(1 - P_{\mathrm{idle}}\right)\cdot t_{to}, \end{aligned} \tag{34}$$

Where t_{to} is the operation duration of S_{HS_i}.

By assuming the energy consumptions of different SBSs to be *i.i.d.*, the energy consumed by the small cell network

restricted in CR_i is

$$E_{\mathrm{HS}_i} = \left(\sum_{v_m=1}^{v_n} \sum_{v_n=1}^{C} v_m \pi\left(v_m, v_n\right) \frac{\frac{p_t}{\eta_{\mathrm{pa}}} + p_{\mathrm{rf}} + p_{\mathrm{bb}}}{(1-\sigma_{\mathrm{dc}})(1-\sigma_{\mathrm{ms}})} + p_{\mathrm{st}} \right) \times N_S\left(i\right) \cdot \left(1 - P_{\mathrm{idle}}\right) \cdot t_{to}. \tag{35}$$

Thus, the network energy consumption of the small cell network in the QN system is

$$E_{\mathrm{QN}} = \sum_{i=1}^{N_p} \left(\sum_{v_m=1}^{v_n} \sum_{v_n=1}^{C} v_m \pi\left(v_m, v_n\right) \frac{\frac{p_t}{\eta_{\mathrm{pa}}} + p_{\mathrm{rf}} + p_{\mathrm{bb}}}{(1-\sigma_{\mathrm{dc}})(1-\sigma_{\mathrm{ms}})} + p_{\mathrm{st}} \right) \times N_S\left(i\right) \cdot \left(1 - P_{\mathrm{idle}}\right) \cdot t_{to}. \tag{36}$$

By combining (30) and (34), the energy efficiency of S_{HS_i} will be (48).

By combining (31) and (35), the network energy efficiency restricted in CR_i is (38).

Based on (32) and (36), the energy efficiency of the small cell network in the QN system is (39).

IV. Numerical and Simulation Results

Based on our proposed 5G ultra-dense small cell network model in this paper, the numerical and simulation results are shown in this section. Some default parameters are configured as $l_i = 1\,\mathrm{km}$, $\zeta = 0.1$, $\alpha_p = 4$, $\rho_0 = 100$, $\eta = 1$, $p_s = 0.01$, $C = 10$, $p_t = 1.6\,\mathrm{W}$, $\eta_{\mathrm{pa}} = 8$, $p_{\mathrm{rf}} = 0.7\,\mathrm{W}$, $p_{\mathrm{bb}} = 1.6\,\mathrm{W}$, $p_{\mathrm{st}} = 6.8\,\mathrm{W}$, $\sigma_{\mathrm{dc}} = 0.08$, $\sigma_{\mathrm{ms}} = 0.1$. Without loss of generality, the centers of hot spots are uniformly distributed in $\mathbb{A}_T$. AEs of hot spots are configured to be *i.i.d.* Poisson distributed with expectation 3000. The ratio of the stationary user density to the SBS density in CR_i is $\theta_i = \frac{\overline{P_i}}{v_n(i)}$.

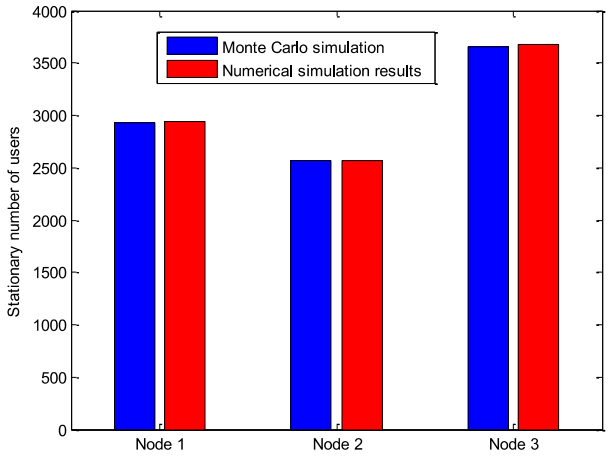

Fig. 4. Comparison between theoretical results and simulation for the stationary number of users in a hot spot.

Comparison of the stationary number of users in a hot spot between numerical results and Monte Carlo simulation is shown in Fig. 4. Three hot spots are selected from $N_p = 50$ hot spots to make this comparison. It is observed from the figure that gaps between Monte carlo simulation and numerical results are very small, indicating that using queueing network theory to extend the R&A model to the temporal domain for the analysis of user density is practicable.

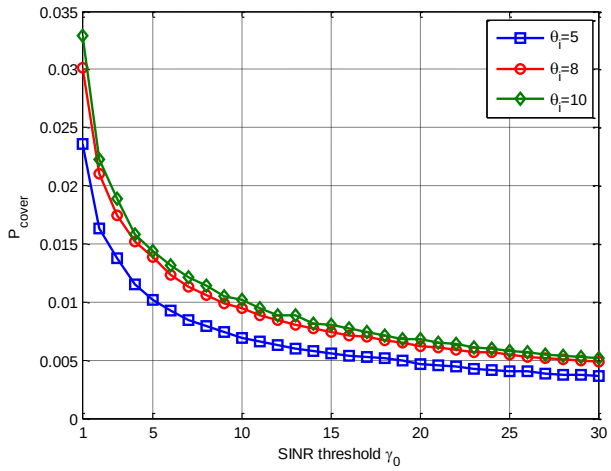

Fig. 5. Coverage probability with respect to the SINR threshold γ_0 considering different ratios of the stationary user density to the SBS density θ_i.

The impact of the SINR threshold γ_0 and the ratio θ_i

$$EE_s = \frac{\left(\int_{x=\gamma_0}^{\infty} \log_2(x+1) f_\lambda(x)\, dx\right) \sum_{v_m=0}^{v_n} \sum_{v_n=0}^{C} v_m \pi(v_m, v_n)}{\left(\sum_{v_m=1}^{v_n} \sum_{v_n=1}^{C} v_m \pi(v_m, v_n) \frac{\frac{p_t}{\eta_{\text{pa}}} + p_{\text{rf}} + p_{\text{bb}}}{(1-\sigma_{\text{dc}})(1-\sigma_{\text{ms}})} + p_{\text{st}}\right)(1 - P_{\text{idle}})}. \tag{48}$$

$$EE_{\text{HS}_i} = \frac{N_S(i)\left(\int_{x=\gamma_0}^{\infty} \log_2(x+1) f_\lambda(x)\, dx\right) \sum_{v_m=0}^{v_n} \sum_{v_n=0}^{C} v_m \pi(v_m, v_n)}{N_S(i)\left(\sum_{v_m=1}^{v_n} \sum_{v_n=1}^{C} v_m \pi(v_m, v_n) \frac{\frac{p_t}{\eta_{\text{pa}}} + p_{\text{rf}} + p_{\text{bb}}}{(1-\sigma_{\text{dc}})(1-\sigma_{\text{ms}})} + p_{\text{st}}\right)(1 - P_{\text{idle}})}. \tag{38}$$

$$EE_{\text{QN}} = \frac{\sum_{i=1}^{N_p} N_S(i)\left(\int_{x=\gamma_0}^{\infty} \log_2(x+1) f_\lambda(x)\, dx\right) \sum_{v_m=0}^{v_n} \sum_{v_n=0}^{C} v_m \pi(v_m, v_n)}{\sum_{i=1}^{N_p} N_S(i)\left(\sum_{v_m=1}^{v_n} \sum_{v_n=1}^{C} v_m \pi(v_m, v_n) \frac{\frac{p_t}{\eta_{\text{pa}}} + p_{\text{rf}} + p_{\text{bb}}}{(1-\sigma_{\text{dc}})(1-\sigma_{\text{ms}})} + p_{\text{st}}\right)(1 - P_{\text{idle}})}. \tag{39}$$

on the coverage probability P_{cover} is investigated in Fig. 5. Fig. 5 shows that when γ_0 is fixed the coverage probability P_{cover} decreases when increasing θ_i. When θ_i is fixed, the coverage probability P_{cover} decreases with the increase of γ_0. The observations is consistent with the results in [3], [32].

number of SBSs in a VC $\overline{N_{\text{cover}}}$ is evaluated in Fig. 6. Fig. 6 reveals that when γ_0 is fixed $\overline{N_{\text{cover}}}$ decreases with the increase of θ_i. When θ_i is fixed, $\overline{N_{\text{cover}}}$ decreases with the increase of the SINR threshold γ_0. Similar results are observed in [3].

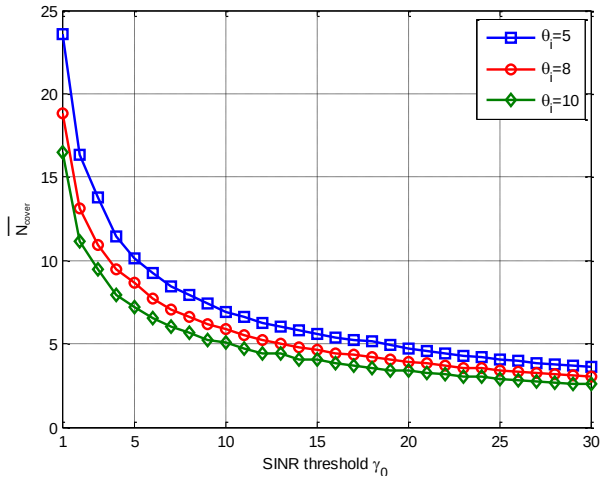

Fig. 6. Average number of SBSs in a VC with respect to the SINR threshold γ_0 considering different ratios of the stationary user density to the SBS density θ_i.

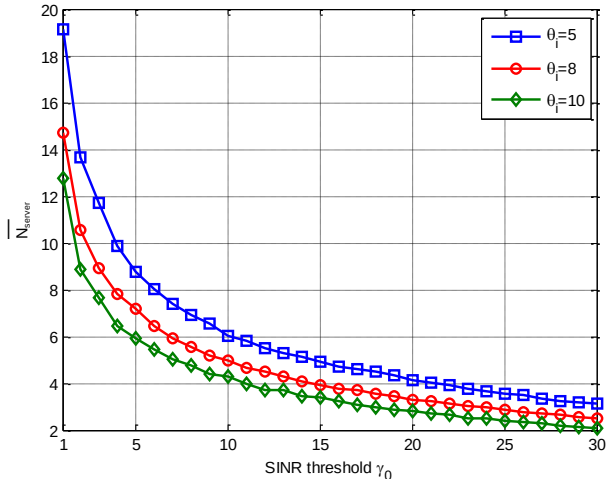

Fig. 7. Average number of available SBSs in a VC with respect to the SINR threshold γ_0 considering different ratios of the stationary user density to the SBS density θ_i.

The effect of the SINR threshold γ_0 and the ratio of the stationary user density to the SBS density θ_i on the average

The influence of the SINR threshold γ_0 and the ratio θ_i on the number of average available SBSs in a VC $\overline{N_{\text{server}}}$

is shown in Fig. 7. As the figure shows, when γ_0 is fixed, $\overline{N_{\text{server}}}$ decreases with the increase of θ_i. When θ_i is fixed, $\overline{N_{\text{server}}}$ decreases with the increase of γ_0. By comparing Fig. 6 with Fig. 7, we find that when γ_0 and θ_i are configured to be the same, $\overline{N_{\text{server}}}$ in Fig. 6 is always smaller than $\overline{N_{\text{cover}}}$ in Fig. 5, due to the limited service capability of SBSs.

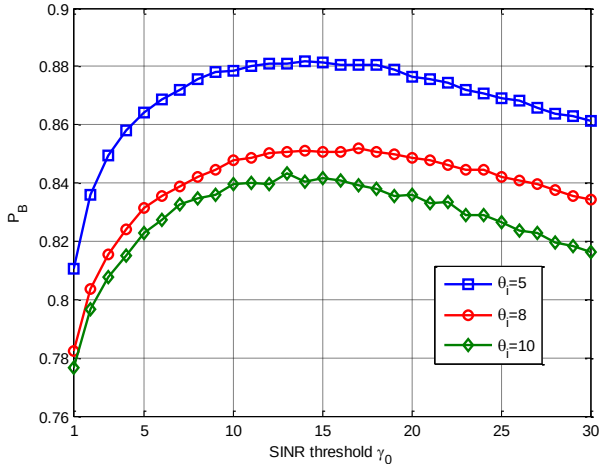

Fig. 8. Blocking probability P_B with respect to the SINR threshold γ_0 considering different ratios of the stationary user density to the SBS density θ_i.

The effect of the SINR threshold γ_0 and the ratio θ_i on the blocking probability P_B is shown in Fig. 8. When γ_0 is fixed, the blocking probability P_B decreases with the increase of θ_i. When θ_i is fixed, the blocking probability P_B first increases with the increase of the SINR threshold γ_0. When the SINR threshold γ_0 is larger than a given threshold, the blocking probability P_B decreases with the increase of the SINR threshold γ_0.

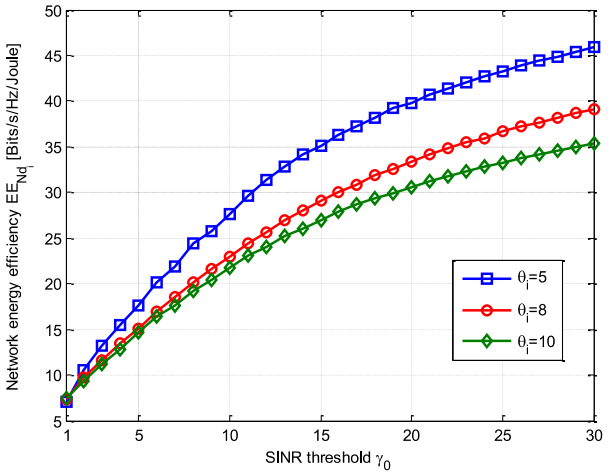

Fig. 9. Network energy efficiency EE_{HS_i} with respect to the SINR threshold γ_0 considering different ratios of the stationary user density to the SBS density θ_i.

The impact of the SINR threshold γ_0 and the ratio θ_i on the network energy efficiency is illustrated in Fig. 9. As the figure shows, when θ_i is fixed, the network energy efficiency EE_{HS_i} increases with the increase of γ_0. Moreover, when the SINR threshold γ_0 is fixed, the network energy efficiency EE_{HS_i} decreases with the increase of θ_i.

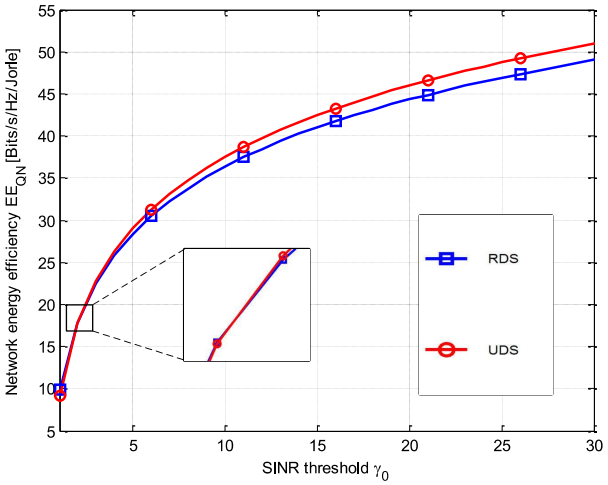

Fig. 10. Network energy efficiency EE_{QN} with respect to the SINR threshold γ_0 for different SBS deploying strategies.

The impact of the SINR threshold γ_0 and the ratio θ_i on the energy efficiency of the small cell network contained in

the QN system is shown in Fig. 10. The user density based deploying strategy (UDS) is implemented by deploying 1000 SBSs into 10 hot spots based on the stationary number of users in each hot spot (e. g. the ratio of user density to base station density is the same for each hot spot), and the randomly deploying strategy (RDS) is implemented by letting SBSs and users be randomly and uniformly distributed in each hot spot without considering R&A model. As the figure shows when $1 < \gamma_0 < 2.2$, energy efficiency of the network based on the RDS is larger than that based on the UDS. When $\gamma_0 > 2.2$, the UDS based network energy efficiency becomes larger than the RDS based network energy efficiency.

V. Conclusion

Based on the R&A model, the impact of the non-uniformly distributed users on performance of 5G ultra-dense small cell networks is firstly investigated in this paper. Moreover, the queueing network theory is firstly adopted to extend the analysis of R&A model to the temporal domain. Based on the theoretical analysis results for the stationary number of users, the coverage probability and the blocking probability are evaluated. Furthermore, by adopting virtual cell technology, the theoretical analyses of the throughput and the energy efficiency for each hot spot are proposed. By the simulations of the proposed model, we observe that when the virtual cell technology is adopted, the network energy efficiency is complicatedly coupled other than varying monotonically with the ratio of the stationary user density to the SBS density. This result provides insights into the important issues such as the optimal deployment of SBSs.

VI. Appendix

A. Coverage probability

The Laplace transform of the random variable Z is denoted by $\mathcal{L}_Z(\varepsilon)$, where Z is

$$Z = \frac{1}{\rho_0 G_s} + \frac{\sum_{i=0}^{N_S(i)(1-P_{\text{cover}})} G_i R_i^{-\alpha_p}}{G_s R_s^{-\alpha_p}}. \tag{41}$$

Thus, the Laplace transform $\mathcal{L}_Z(\varepsilon)$ is derived as (42), where $\exp(\cdot)$ is the exponential function and $\mathbb{E}_{G_s,G_i,R_s,R_i}(\cdot)$ is the expectation operations on random variables G_s, G_i, R_s and R_i.

And the PDFs of G_s, G_i, R_s and R_i are

$$\begin{cases} f_{G_s}(x) = \eta \exp(-\eta x) \\ f_{G_i}(x) = \eta \exp(-\eta x) \\ f_{R_s}(x) = \frac{4x}{\pi l_i^2}\left(\arccos\frac{x}{2l_i} - \frac{x}{2l_i}\sqrt{1-\frac{x^2}{4l_i^2}}\right) \\ f_{R_i}(x) = \frac{4x}{\pi l_i^2}\left(\arccos\frac{x}{2l_i} - \frac{x}{2l_i}\sqrt{1-\frac{x^2}{4l_i^2}}\right) \end{cases}. \tag{43}$$

Based on (6)(42)(43), the Laplace transform of Z is further derived by (43).

with (44).

By substituting (42) (44) into (43), the Laplace transform in (43) becomes (45).

Similar to [34], by the Euler summation on (45), P_{cover} becomes

$$\mathcal{L}_Z(\varepsilon)=\mathbb{E}_{G_s,G_i,R_s,R_i}\left(\exp\left(-\varepsilon\left(\frac{1}{\rho_0 G_s}+\frac{\sum_{i=0}^{N_S(i)(1-P_{\text{cover}})}G_iR_i^{-\alpha_p}}{G_sR_s^{-\alpha_p}}\right)\right)\right), \tag{42}$$

$$\begin{aligned}\mathcal{L}_Z(\varepsilon)&=\mathbb{E}_{G_s,G_i,R_s,R_i}\left(\exp\left(-\varepsilon\left(\frac{1}{\rho_0 G_s}+\frac{\sum_{i=0}^{N_S(i)(1-P_{\text{cover}})}G_iR_i^{-\alpha_p}}{G_sR_s^{-\alpha_p}}\right)\right)\right)\\&=\mathbb{E}_{G_s,G_i,R_s,R_i}\left(\exp\left(\frac{-\varepsilon}{\rho_0 G_s}\right)\prod_{i=0}^{N_S(i)(1-P_{\text{cover}})}\exp\left(\frac{-\varepsilon G_iR_i^{-\alpha_p}}{G_sR_s^{-\alpha_p}}\right)\right)\\&=\mathbb{E}_{G_s}\left(\exp\left(\frac{-\varepsilon}{\rho_0 G_s}\right)\cdot\left(\mathbb{E}_{G_i,R_s,R_i}\left(\exp\left(\frac{-\varepsilon G_iR_i^{-\alpha_p}}{G_sR_s^{-\alpha_p}}\right)\right)\right)^{N_S(i)(1-P_{\text{cover}})}\right)\\&=\int_0^\infty\exp\left(\frac{-\varepsilon}{\rho_0 G_s}\right)(\eta\exp(-\eta G_s))\cdot\left(\mathbb{E}_{G_i,R_s,R_i}\left(\exp\left(\frac{-\varepsilon G_iR_i^{-\alpha_p}}{G_sR_s^{-\alpha_p}}\right)\right)\right)^{\overline{N_{\text{int}}}}dG_s\\&=\int_0^\infty\eta\exp\left(\frac{-\varepsilon}{\rho_0 G_s}-\eta G_s\right)\left(\mathbb{E}_{G_i,R_s,R_i}\left(\exp\left(\frac{-\varepsilon G_iR_i^{-\alpha_p}}{G_sR_s^{-\alpha_p}}\right)\right)\right)^{\overline{N_{\text{int}}}}dG_s,\end{aligned} \tag{43}$$

$$\begin{aligned}\mathbb{E}_{G_i,R_s,R_i}\left(\exp\left(\frac{-\varepsilon G_iR_i^{-\alpha_p}}{G_sR_s^{-\alpha_p}}\right)\right)=&\int_0^{2l_0}\int_0^{2l_0}\int_0^\infty\exp\left(\frac{-\varepsilon G_iR_i^{-\alpha_p}}{G_sR_s^{-\alpha_p}}\right)\cdot\\&\left(f_{G_i}(G_i)\,f_{R_s}(R_s)\,f_{R_i}(R_i)\right)dG_idR_sdR_i,\end{aligned} \tag{44}$$

$$\begin{aligned}\mathcal{L}_Z(\varepsilon)=&\mathbb{E}_{G_0}\left(\exp\left(-\frac{\varepsilon}{\rho_0 G_s}\right)\int_0^\infty\int_0^{2l_i}\int_0^{2l_i}\exp\left(\frac{-\varepsilon G_iR_i^{-\alpha_p}}{G_sR_s^{-\alpha_p}}\right)\left(\frac{4R_s}{\pi l_i^2}\left(\arccos\frac{R_s}{2l_i}-\frac{R_s}{2l_i}\sqrt{1-\frac{{R_s}^2}{4l_i^2}}\right)\right)\cdot\right.\\&\left.\left(\frac{4R_i}{\pi l_i^2}\left(\arccos\frac{R_i}{2l_i}-\frac{R_i}{2l_i}\sqrt{1-\frac{{R_i}^2}{4l_i^2}}\right)\right)(\eta\exp(-\eta G_i))\,dG_idR_sdR_i\right)^{\overline{N_{\text{int}}}}\Bigg)\\=&\int_0^\infty\left(\eta\exp\left(-\frac{\varepsilon}{\rho_0 G_s}-\eta G_s\right)\int_0^\infty\int_0^{2l_i}\int_0^{2l_i}\exp\left(\frac{-\varepsilon G_iR_i^{-\alpha_p}}{G_sR_s^{-\alpha_p}}\right)\left(\frac{4R_s}{\pi l_i^2}\left(\arccos\frac{R_s}{2l_i}-\frac{R_s}{2l_i}\sqrt{1-\frac{{R_s}^2}{4l_i^2}}\right)\right)\cdot\right.\\&\left.\left(\frac{4R_i}{\pi l_i^2}\left(\arccos\frac{R_i}{2l_i}-\frac{R_i}{2l_i}\sqrt{1-\frac{{R_i}^2}{4l_i^2}}\right)\right)(\eta\exp(-\eta G_i))\,dG_idR_sdR_i\right)^{\overline{N_{\text{int}}}}\Bigg)dG_s.\end{aligned} \tag{45}$$

$$\begin{aligned}P_{\text{cover}}=&2^{-B_e}\gamma_0\exp\left(\tfrac{A_e}{2}\right)\sum_{b_e=0}^{B_e}\binom{B_e}{b_e}\times\\&\sum_{c_e=0}^{C_e+b_e}\frac{(-1)^{c_e}}{D_e}\mathrm{Re}\left(\frac{\mathcal{L}_Z(\hbar)}{\hbar}\right)\quad.\end{aligned} \tag{46}$$

$$D_e=\begin{cases}2 & \text{if } c_e=0\\ 1 & \text{others}\end{cases}. \tag{47}$$

Based on the analysis in [35], A_e, B_e and C_e should be no less than $t\ln 10$, $1.243t-1$ and $1.467t$ respectively to obtain a numerical accuracy of 10^{-t}. In this paper, A_e, B_e and C_e are configured to be $8\ln 10$, 11 and 14 in order to obtain a numerical accuracy of 10^{-9} for the theoretical analysis. The parameter $\hbar$ is expressed as $\hbar=\left(A_e+2\pi c_eJ\right)/\left(2\gamma_0^{-1}\right)$, where J is the imaginary unit and $\mathrm{Re}(\cdot)$ denotes the real part of the given variable in parentheses. The parameter D_e is

By substituting (45) into (46), the coverage probability P_{cover} becomes (12).

REFERENCES

[1] P. Demestichas, et al., "5G on the horizon: Key challenges for the radioaccess network," *IEEE Veh. Technol. Mag.*, vol. 8, no. 3, pp. 47–53, Sep. 2013.

[2] J. G. Andrews, et al., "What will 5G be?" *IEEE J. Sel. Areas Commun.*, vol. 32, no. 6, pp. 1065–1082, Jun. 2014.

[3] X. Ge, J. Ye, Y. Yang, and Q. Li, "User mobility evaluation for 5G small cell networks based on individual mobility model," *IEEE J. Sel. Areas Commun.*, vol. 34, no. 3, pp. 528–541, 2016.

[4] X. Ge, S. Tu, G. Mao, C.-X. Wang, and T. Han, "5G ultra-dense cellular networks," *IEEE Wireless Commun.*, vol. 23, no. 1, pp. 72–79, Feb. 2016.

[5] G. Wu et al., "Recent advances in energy-efficient networks and their application in 5G systems," *IEEE Wireless. Commun.*, vol. 22, no. 2, pp. 145–151, Apr. 2015.

[6] S. Stefanatos, and A. Alexiou, "Access point density and bandwidth partitioning in ultra dense wireless networks," IEEE Trans. Commun., vol. 62, no. 9, pp. 3376-3384, Sep. 2014.

[7] S. Samarakoon, et al. , "Ultra Dense Small Cell Networks: Turning Density into Energy Efficiency," *IEEE J. Sel. Areas Commun.*, vol.34, no. 5, pp. 1267–1280, May. 2016.

[8] D. Lpez-Prez, M. Ding, H. Claussen, and A. H. Jafari, "Towards 1 Gbps/UE in cellular systems: Understanding ultra-dense small cell deployments," *IEEE Commun. Surveys and Tutorials.*, vol. 17, no. 4, pp. 2078–2101, Jun. 2015.

[9] F. Tseng, L. Chou, H. Chao, and J. Wang, "Ultra-dense small cell planning using cognitive radio network toward 5G," *IEEE Wireless. Commun.*, vol. 22, no. 6, pp. 76–83, Dec. 2015.

[10] F. Zhou, N. C. Beaulieu, Z. Li, J. Si, and P. Qi, "Energy-efficient optimal power allocation for fading cognitive radio channels: ergodic capacity, outage capacity and minimum-rate capacity," *IEEE Trans. Wireless Commun.*, vol. 15, no. 4, pp. 2741–2755, Apr. 2016.

[11] Y. Zhong, T. Q. S. Quek and X. Ge, "Heterogeneous cellular networks with spatio-temporal traffic: delay analysis and scheduling," *IEEE J. Sel. Areas Commu.*, early access.

[12] T. Zhang, J. Zhao, L. An, and D. Liu, "Energy efficiency of base station deployment in ultra dense HetNets: a stochastic geometry analysis," *IEEE Wireless Commun. Letters*, vol. 5, no. 2, pp. 184–187, Apr. 2016.

[13] M. Ding, P. Wang, D. Lpez-Prez, G. Mao, and Z. Lin, "Performance impact of LoS and NLoS transmissions in dense cellular networks," *IEEE Trans. Wireless Commun.*, vol. 15, no. 3, pp. 2365–2380, Mar. 2016.

[14] S. F. Yunas, M. Valkama, and J. Niemel, "Spectral and energy efficiency of ultra-dense networks under different deployment strategies," *IEEE Wireless Commun. Mag.*, vol. 53, no. 1, pp. 90–100, Jan. 2015.

[15] J. Park, S.L. Kim, and J. Zander, "Tractable resource management with uplink decoupled millimeter-wave overlay in ultra-dense cellular networks," *IEEE Trans. Wireless Commun.*, vol. 15, no. 6, pp. 4362–4379, Jun. 2016.

[16] Z. Gao, et al., "Mmwave massive MIMO based wireless backhaul for 5G ultra-dense network," *IEEE Wireless Commun.*, vol. 22, no. 5, pp. 13–21, Oct. 2015.

[17] O. Galinina, A. Pyattaev, S. Andreevy, M. Dohler, and Y. Koucheryavy, "5G multi-RAT LTE-WiFi ultra-dense small cells: Performance dynamics, architecture, and trends," *IEEE J. Sel. Areas Commun.*, vol. 33, no. 6, pp. 1224–1240, May 2015.

[18] A. Ghazanfari, H. Tabassum, and E. Hossain, "Ambient RF energy harvesting in ultra-dense small cell networks: performance and tradeoffs," *IEEE Wireless Commun.*, vol. 23, no. 2, pp. 38–45, May. 2016.

[19] Q. Wu, M. Tao, D. W. K. Ng, W. Chen, and R. Schober, "Energy-efficient resource allocation for wireless powered communication networks," *IEEE Trans. Wireless Commun.*, vol. 15, no. 3, pp. 2312–2327, March. 2016.

[20] S. Chen, F. Qin, B. Hu, X. Li, and Z. Chen, "User-centric ultra-dense networks for 5G: Challenges, methodologies, and directions," *IEEE Wireless Commun.*, vol. 23, no. 2, pp. 78–85, Apr. 2016.

[21] J. Kim, H.-W. Lee, and S. Chong, "Virtual cell beamforming in cooperative networks," *IEEE J. Sel. Areas Commun.*, vol. 32, no. 6, pp. 1126–1138, Jun. 2014.

[22] J. Wang, and L. Dai, "Downlink rate analysis for virtual-cell based large-scale distributed antenna systems," *IEEE Trans. Wireless Commun.*, vol. 15, no. 3, pp. 1998–2011, Mar. 2016.

[23] W. Nie, F. Zheng, X. Wang, W. Zhang, and S. Jin, "User-centric cross-tier base station clustering and cooperation in heterogeneous networks: rate improvement and energy saving," *IEEE J. Sel. Areas Commun.*, vol. 34, no. 5, pp. 1192–1206, May. 2016.

[24] M. Hong, R. Sun, H. Baligh, and Z. Q. Luo, "Joint base station clustering and beamformer design for partial coordinated transmission in heterogeneous networks," *IEEE J. Sel. Areas Commun.*, vol. 31, no. 2, pp. 226–240, Feb. 2013.

[25] C. Li, J. Zhang, M. Haenggi, and K. B. Letaief, "User-centric intercell interference nulling for downlink small cell networks," *IEEE Trans. Commun.*, vol. 63, no. 4, pp. 1419–1431, Apr. 2015.

[26] C. Song, et al, "Limits of Predictability in Human Mobility, *Science*, vol. 327, pp. 1018-21, Feb. 2010.

[27] C. Song et al., "Modeling the Scaling Properties of Human Mobility," *Nature Physics*, vol. 6, pp. 818–823, Sept. 2010.

[28] G. K. Zipf, "The P1P2/D hypothesis: on the intercity movement of persons," *Am. Sociol. Rev.*, vol. 11, pp. 677–686, 1946.

[29] F Simini, et al., "A universal model for mobility and migration patterns," *Nature*, vol. 484, no. 7392, pp. 96, 2012.

[30] J. Jackson, "Networks of waiting lines," *Operations research*, vol. 5, no. 4, pp. 518–521, 1954.

[31] L. A. Santalo, "Integral geometry and geometric probability," *Encyclopedia of Mathematics and its Applications*, vol.1, 1976.

[32] X. Ge et al., "Spatial spectrum and energy efficiency of random cellular networks," *IEEE Trans. Commun.*, vol. 63, no. 3, pp. 1019–1030, Mar. 2015.

[33] J. Guo, S. Durrani, and X. Zhou, "Outage probability in arbitrarily-shaped finite wireless networks," *IEEE Trans. Commun.*, vol. 62, no. 2, pp. 699–712, Feb. 2014.

[34] J. Abate and W. Whitt, "Numerical inversion of Laplace transforms of probability distributions," *ORSA J. Compt.*, vol. 7, no. 1, pp. 36–43, 1995.

[35] C. A. OCinneide, "Euler summation for Fourier series and Laplace transform inversion," *Commun. Statist. Stochastic Models*, vol. 13, no. 2, pp. 315–337, 1997.

[36] M. Imran, et al., "Energy Efficiency Analysis of The Reference Systems, Areas of Improvements and Target Breakdown," *Tech. Rep. ICT-EARTH deliverable*, Tech. Rep, 2011.